Hindawi Publishing Corporation
Advances in Mechanical Engineering
Volume 2013, Article ID 474935, 8 pages
http://dx.doi.org/10.1155/2013/474935

Research Article

Simulation and Experimental Investigation of Thermal Performance of a Miniature Flat Plate Heat Pipe

R. Boukhanouf[1] and A. Haddad[2]

[1] *Department of the Built Environment, University of Nottingham, Nottingham NG7 2RD, UK*
[2] *FrigoDynamics GmbH, Bahnhofstraße 16, 85570 Markt Schwaben, Germany*

Correspondence should be addressed to R. Boukhanouf; rabah.boukhanouf@nottingham.ac.uk

Received 4 February 2013; Accepted 25 March 2013

Academic Editor: Godson Asirvatham Lazarus

This paper presents the results of a CFD analysis and experimental tests of two identical miniature flat plate heat pipes (FPHP) using sintered and screen mesh wicks and a comparative analysis and measurement of two solid copper base plates 1 mm and 3 mm thick. It was shown that the design of the miniature FPHP with sintered wick would achieve the specific temperature gradients threshold for heat dissipation rates of up to 80 W. The experimental results also revealed that for localised heat sources of up to 40 W, a solid copper base plate 3 mm thick would have comparable heat transfer performances to that of the sintered wick FPHP. In addition, a marginal effect on the thermal performance of the sintered wick FPHP was recorded when its orientation was held at 0°, 90°, and 180° and for heat dissipation rates ranging from 0 to 100 W.

1. Introduction

Conventional heat sink-fan air coolers in electronics packages are becoming inadequate for use in faster, compact, and more powerful multitasked microprocessors that generate large quantities of attendant heat. This has led current research to focus on high-performance and compact thermal solutions [1]. Heat pipes have been extensively researched and applied in various embodiments for electronics cooling ranging from simple cylindrical geometries to complex configurations [2]. FPHPs in particular have high-heat transfer capability, can maintain a uniform temperature over the evaporator surface when densely packed with heat-generating components, and decrease the thickness of finned heat sinks base material [3–6].

Recent research by Christensen and Graham [7] investigated the performance of heat sinks in packaging high-power (>1 W) light-emitting diode (LED) arrays and concluded that flat plate heat pipes form an important thermal component to achieve long operating life and high reliability. Huang and Liu [8] demonstrated analytically the increased capability of mounting a localised heat source and heat sink on the same surface of an FPHP. Similarly, Qin and Liu [9] investigated liquid flow in an anisotropic permeability wick of a flat plate heat pipe, determining the effect of heat source location on fluid distribution in the inside of the heat pipe. Further work on finding the optimum location of mounting multiple heat sources on an FPHP evaporator surface was demonstrated by Tan et al. [10] through a simplified analytical solution to a two-dimensional pressure and velocity distribution within the wick. Recently, Sonan et al. [11] developed a simulation model for the transient thermal performance of a 40 × 40 × 0.9 mm FPHP with specific applications to cooling multiple electronics components where space restriction imposes that heat sources and heat sinks need to be mounted on the same surface. The above research agrees that a cost premium associated with a well-designed FPHP for advanced thermal management solution in electronics cooling should be reflected in its superior thermal performance compared to solid copper or aluminium base materials of similar dimensions.

This paper investigates the design and thermal performance of a miniature FPHP as an effective supporting shelf for printed circuit boards (PCB) of radio frequency (RF)

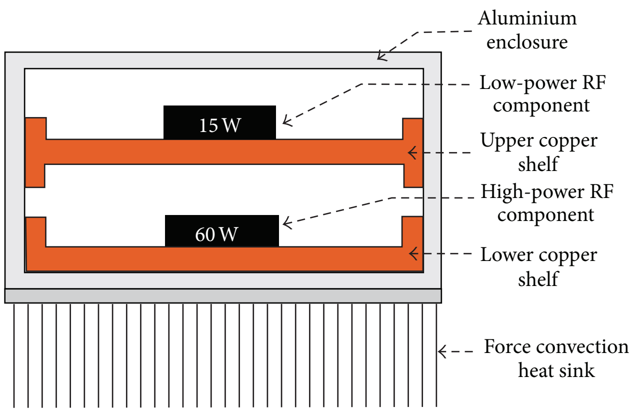

FIGURE 1: Schematic of the electronics cooling enclosure.

components to dissipate and transport heat away to the aluminium enclosure. In this paper, two identical miniature FPHPs configurations one with a sintered copper powder and the other one with a screen copper mesh wick were designed and tested. A further benchmarking exercise, using both CFD analysis and experimental measurements, was carried out by comparing the thermal performance of the FPHP to that of a monolithic solid copper plate with similar dimensions.

2. Description of the Electronics Enclosure Cooling System

The work addresses the cooling requirement to maintain a specified temperature limit for heat-generating RF components that are housed in an existing aluminium enclosure as part of a large telecommunication control system. The aluminium enclosure consists of two separate copper shelves and an air cooled finned base plate, as shown in Figure 1. The PCB of high heat dissipating RF components was mounted on the lower shelf of the enclosure to allow for direct contact with the base heat metal spreader while low-power rated RF components were placed on the top shelf. In the original design, the enclosure's shelves were made of 1 mm thick copper base. However, frequent and premature failures of RF components prompted the review of the enclosure's thermal performance. Hence, a redesign of the copper shelves to keep the operating temperature gradients of the RF components within the specified limits was performed using both CFD simulation and an experimental validation analysis. The work consists in investigating the thermal performance of the enclosure's shelves that are made of a 1 mm and 3 mm solid copper base plates and two miniature FPHPs of 5 mm overall height with one using sintered copper powder wick and the other one a screen mesh wick.

2.1. FPHP Design. The FPHP base material was made of copper material and water was selected as the working fluid for its compatibility and suitable operating temperature range. The outer shell of the constructed prototype miniature FPHPs for the sintered and mesh wicks is shown in Figure 2(a). The inner structure of the sintered wick FPHP with the condenser cover plate removed to reveal the sintered wick layer and erected pillars on the evaporator surface is shown in Figure 2(b). Similarly, the structure of the miniature FPHP with copper mesh wick is shown in Figure 2(c). The design of the mesh wick FPHP was adopted from Bakke [12] and Rosenfeld et al. [13], which consists of using a fine mesh layer to provide capillary pumping force of the working fluid and a coarse mesh to support and maintain the structural integrity of the vapour space.

2.2. FPHP CFD Simulation. The thermal performance of the miniature FPHP was simulated using FloTHERM, a commercial CFD simulation software. The computer simulation includes analysing the complex flow pattern of the working fluid in the wick and establishing the temperature profiles in the FPHP evaporator. Flotherm is a finite volume-based software package that uses simple Cartesian grid meshing and has built in boundary conditions for common heat transfer devices. The rectangular shape of the FPHP, heater block, and cold plate lend themselves well to meshing using Cartesian coordinates and hence the use of Flotherm for a fast and converging solution. Description of the mathematical model for momentum, mass, and energy conservation that underpin the CFD simulation was not the focus of this paper as similar models are widely available in published literature that can be found in [14–16].

The Flotherm model was built using standard Cuboids and Prism elements for the FPHP components including the evaporator and condenser copper plates, the wick layer, the void (vapour) space, and the supporting solid columns. Planar resistance object model was used to define the thermal properties for each object. This is a useful tool where the thermal resistance of an object can be inserted manually or determined from other thermal parameters such as the thermal conductivity and heat transfer coefficient. Modelling of the porous wick layer, in particular, requires prior knowledge of the permeability of the porous wick structure. The volumetric flow rate, $\dot{V}$, of the working fluid was also required as an input parameter in the simulation. This was calculated from the following relationship:

$$\dot{V} = \frac{\dot{Q}_H}{\rho_l h}, \tag{1}$$

where $\dot{Q}_H$ is the rate of heat generation in the heat source and h, and ρ_l are the latent heat and density of the working fluid, respectively. In addition, it is well known that the failure of heat pipes is often attributed to operation beyond the device's wick capillary limit. This can be obtained by characterising the actual pressure of the liquid in the wick pores under different heat flux levels using Laplace-Young equation as follows [1]:

$$\Delta p_c = \frac{2\sigma_l}{r_{\text{pore}}}, \tag{2}$$

where Δp_c is the capillary pressure drop in the wick, σ_l is the surface tension of the liquid, and r_{pore} is the pore radius of the wick.

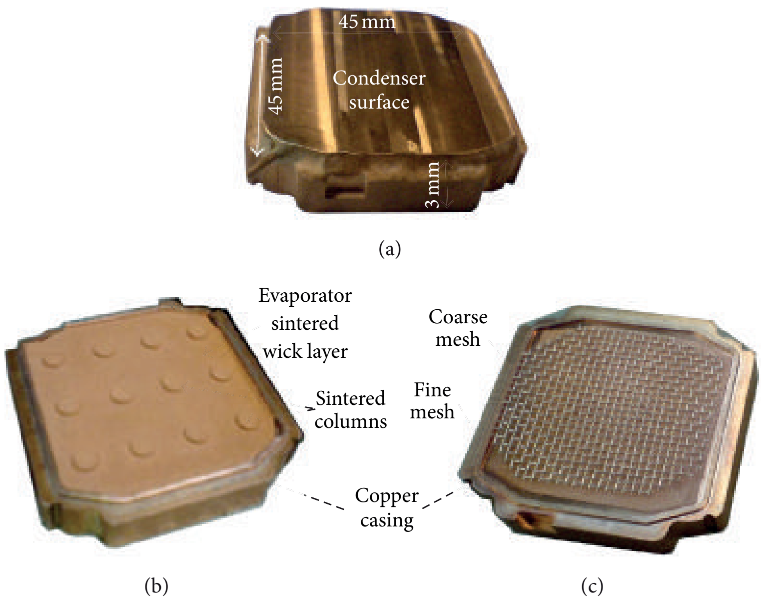

Figure 2: Constructed miniature FPHP (a) sealed unit, (b) sintered wick, and (c) mesh wick.

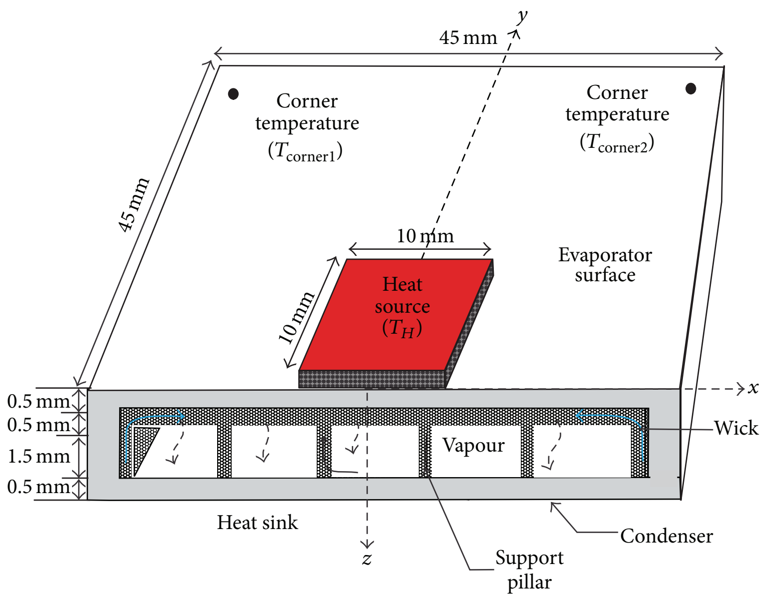

Figure 3: A schematic representation of the FPHP.

Equally, the effective thermal conductivity of a saturated wick, k_{eff}, was obtained from the following expression [17, 18]:

$$k_{eff} = \beta\left(\varphi k_l + (1-\varphi) k_s\right) + \frac{(1-\beta)}{\varphi/k_l + (1-\varphi)/k_s}, \quad (3)$$

where φ is the porosity of the wick, k_l and k_s are the thermal conductivity of liquid water and solid wick, respectively. According to Bhattacharya et al. [17], the best-fit data for measuring the effective thermal conductivity of a porous material is for $\beta = 0.35$ with an overall R^2 value of 0.97. This is consistent with measured thermal conductivities of about 40 W/(mK) in heat pipes with fully saturated wicks, while the vapour space is considered to have a very large heat transfer coefficient of the order of 50000 W/m^{2}K [16, 18].

A schematic representation of the sintered wick heat pipe given in Figure 3 illustrates the location of the heat source, a cross section of the wick layer, the working fluid circulation paths, and the condenser cold plate heat sink.

In this analysis, it was also assumed that the heat source is of constant heat flux type which is applied to the evaporator base plate (at $z = 0$) immediately under the heat source while

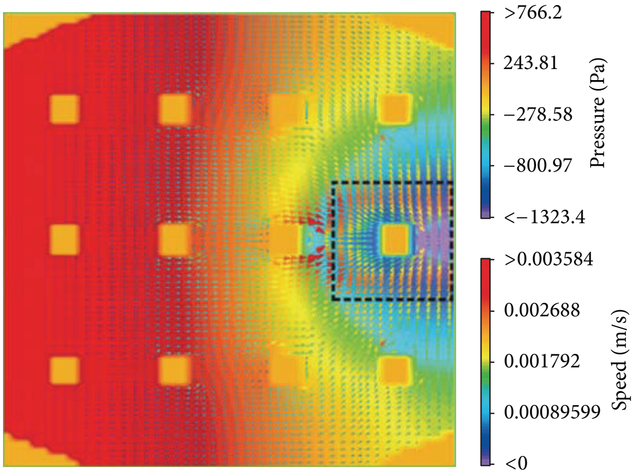

Figure 4: CFD simulation of speed and pressure fields of the liquid in the FPHP-sintered wick ($Q_H = 80$ W).

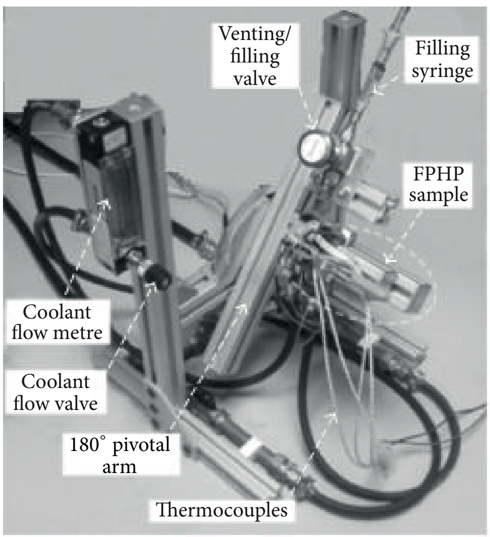

Figure 5: The experimental test rig setup.

the remaining outer surface of the evaporator including the edge walls is considered to be adiabatic. In the inner section of the heat pipe, it was assumed that the liquid-vapour interface temperature is equal to the vapour saturation temperature of the working fluid that can be calculated from Clausius-Clapeyron relationship [19]. Similarly, the liquid velocity at the interface of the wick layer-evaporator wall was assumed to equal zero. At the condenser-vapour interface, the temperature of the condenser section was maintained at 35°C using a chilled liquid cold plate with a heat transfer coefficient in the order of 2000 W/(m^{2}K).

A thermocouple placed at the interface surface between the evaporator and heat source was used to measure the temperature of the heater block, T_H, and a further two thermocouples were placed at the two farthest corners on the evaporator to measure T_{corner1} and T_{corner2}. Furthermore, the heat dissipation from the RF components was simulated

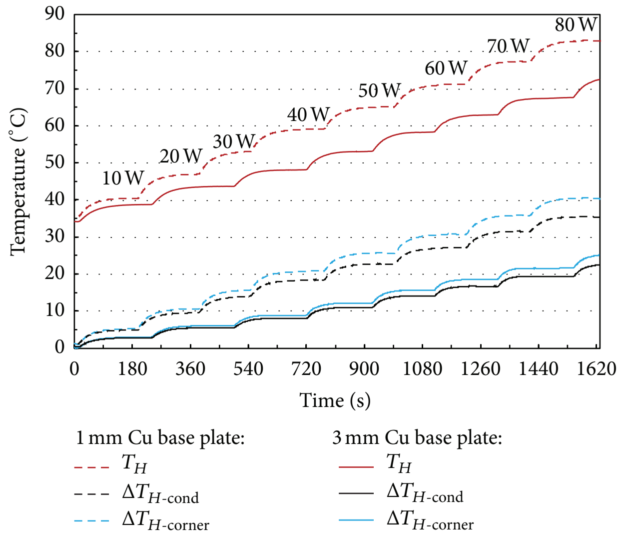

Figure 6: Temperature variation of a 1 mm and 3 mm thick copper base plates.

Table 1: Design properties of the sintered and mesh wick miniature FPHP.

Casing	
Material	Copper
Height	3 mm
Dimension	45 mm × 45 mm
Heater block size	10 mm × 10 mm
Working fluid	Water
Sintered copper powder wick	
Wick thickness	0.5 mm
Vapour space height	1.5 mm
Porosity	50%
Pore radius	40 μm
Permeability	1.43×10^{-11} m^2
Screen copper mesh wick	
Fine mesh material	Phosphor bronze 320 mesh/in
Wire diameter	0.03 mm
Porosity	42%
Wick thickness	1 mm
Supporting coarse mesh material	Phosphor bronze 16 mesh/in

using an electric heater cartridge that is inserted in a solid aluminium block of 10 mm × 10 mm with a controlled heat dissipation rates. The condenser surface was maintained to the desired temperature of 35°C by clamping directly onto its surface a chilled water cold plate. The main design properties of the miniature FPHPs with sintered and mesh wicks are given in Table 1.

2.3. CFD Simulation Results. The CFD simulation was used to evaluate the sintered wick FPHP thermal performance by

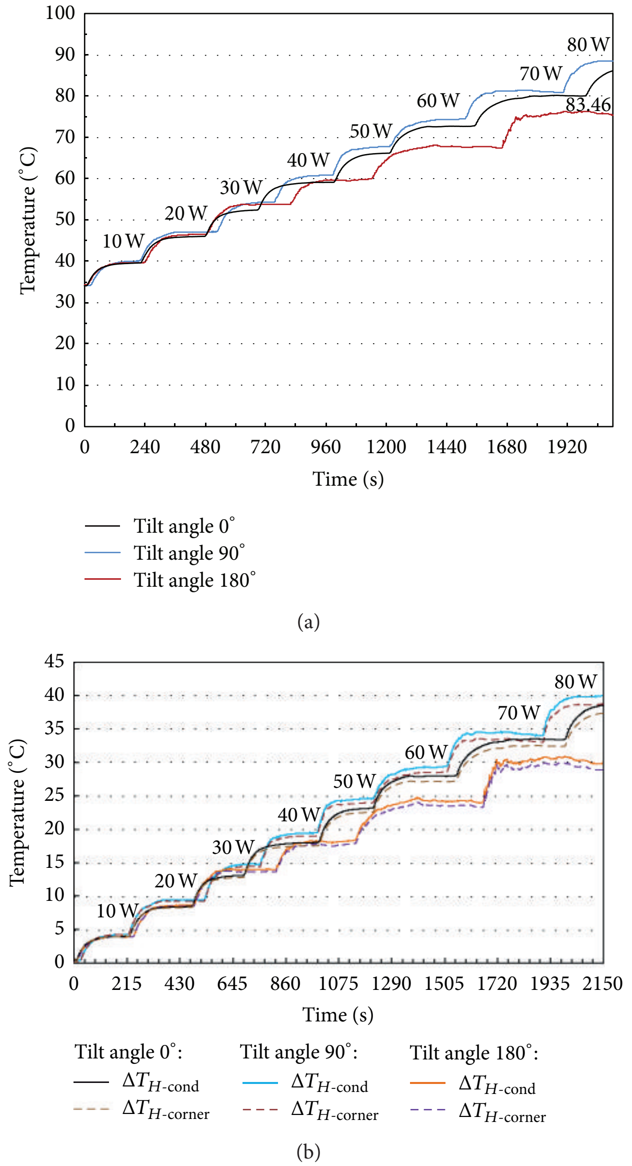

Figure 7: Screen mesh wick FPHP temperature variation at various heat dissipation levels and tilt angles: (a) heat source temperature, (b) evaporator surface temperature gradient.

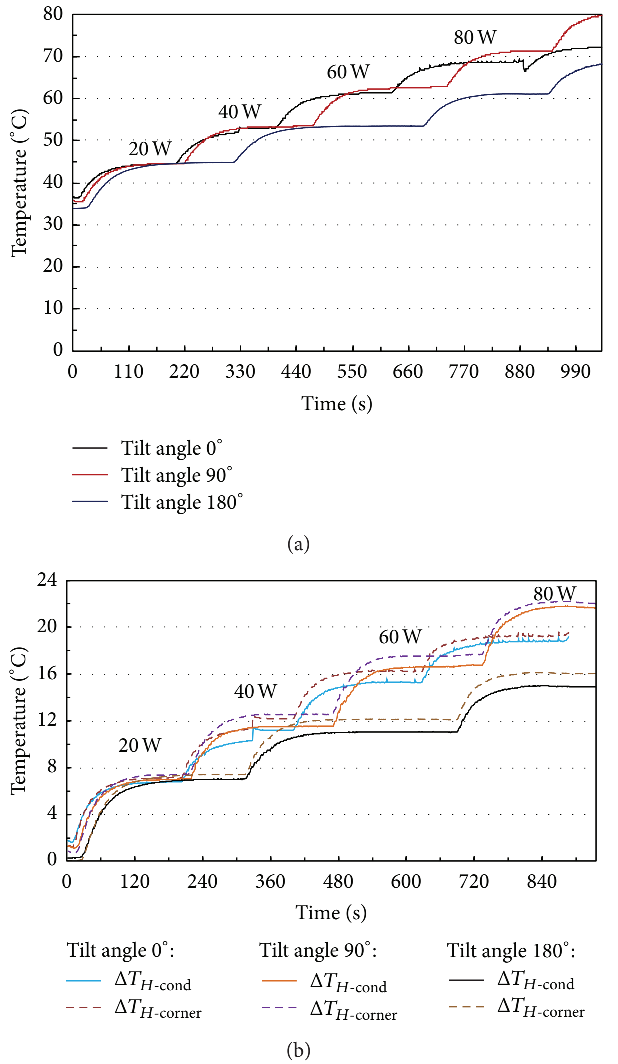

Figure 8: Sintered wick FPHP temperature at various heat dissipation levels and tilt angles: (a) heat source temperature, (b) surface temperature gradient.

analysing the steady state liquid flow pressure and velocity distribution in the sintered wick as shown in Figure 4. The speed of the liquid flow in the wick structure is presented by arrows pointing towards the heat source (dashed line square) and arranged by colour in contours of equal speeds. It can be seen that the speed of the liquid flow is lowest at regions most distant from the heat source (contours of purple arrows) and increases gradually as the liquid is drawn towards the heat source (contours of orange and red arrows) to replenish the evaporated liquid from the wick pores in the constant heat flux section. The liquid flow speed then drops sharply in the region immediately underneath the heat source as the liquid evaporates from the wick. The effect of the sintered pillars is also visible in that the liquid flow speed field contours are altered in a way that high-fluid speed spots were developed around the pillars. Furthermore, Figure 4 shows the liquid pressure distribution in the wick with the high pressure region (in red colour) away from the heat source and the low-pressure regions (in blue/purple colour) immediately beneath the heat source.

From the CFD analysis, it was found that the total pressure difference generated by the capillary forces of the wick is 2089.6 N/m^2. This is markedly lower than the capillarity pumping limit of the wick of 3952 N/m^2 which was calculated using (2) under the working conditions given in Table 2.

3. Experimental Setup and Results

The experimental rig setup to test the thermal performance of the miniature FPHP and solid copper base samples is shown in Figure 5. The rig was equipped with a liquid filling

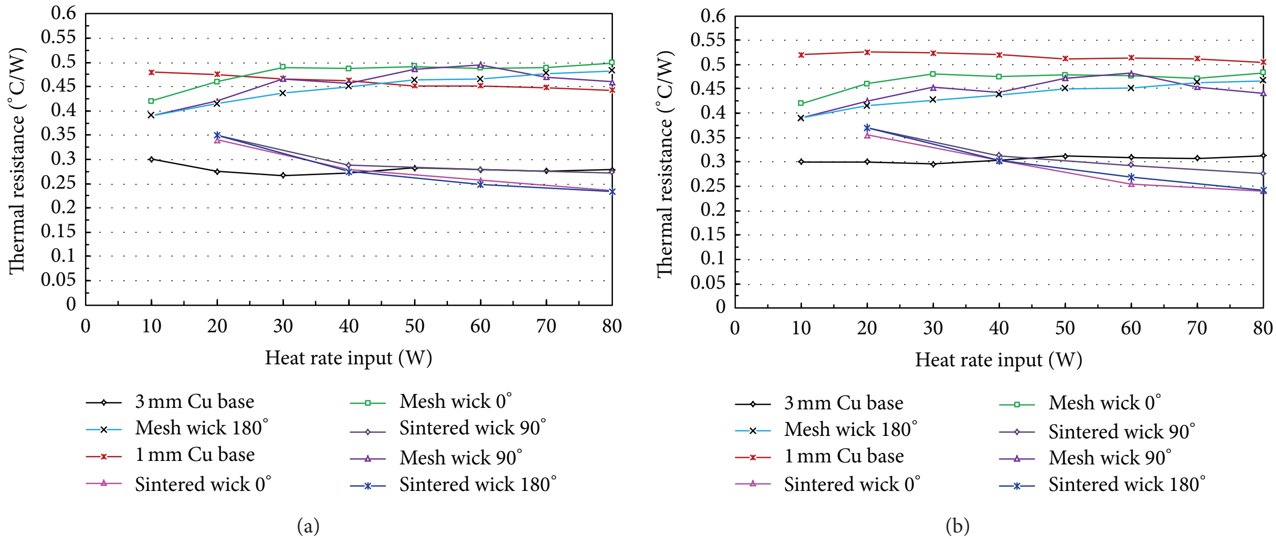

Figure 9: Thermal resistance: (a) one dimensional resistance, (b) spreading resistance.

Table 2: Saturated wick operating properties.

Heat load $\dot{Q}_H$ (W)	Liquid surface tension σ_l (kg/s^2)	Liquid density ρ_l (kg/m^3)	Liquid latent heat of vaporisation h (kJ/kg)	Sintered powder wick permeability $\varepsilon_{\text{wick}}$ (m^2)	Liquid flow rate from (1) $\dot{V}$ (m^3/s)	Pressure drop from (2) ΔP_c (N/m^2)	Pressure drop (CFD) ΔP_{CFD} (N/m^2)
80	0.0626	972	2310	1.43E − 11	3.563E − 08	3952	2089.6

Table 3: Sintered wick FPHP thermal resistance calculation uncertainty.

Heat input (W)	20	40	60	80
Calculated thermal resistance uncertainty (%)	13.60	6.00	4.14	3.80

and venting system for charging the FPHP, a rotating beam for mounting the heat pipe at different tilt angles (0° to 180°), a variable power supply to control heat dissipation from the heat source, a chilled water supply to control the condenser temperature, and associated sensors and data acquisition equipment. The miniature FPHP test sample was clamped onto the tilting beam with 0° angle being designated for operation against gravity (i.e., evaporator is above the condenser). An electric heater cartridge placed inside an aluminium block of 10 mm × 10 mm was used as heat source which heat dissipation rate was controlled by a variable power supply. A thermal interface material 0.5 mm thick was used as an interface between the FPHP test sample, the heater block, and the condenser cold plate to minimise the contact thermal resistances.

The performance of the FPHP test sample was evaluated at various heat dissipation rates by increasing the heat source power at equal increments of 10 W to a maximum of 100 W or until the temperature of the evaporator surface reached a threshold of 100°C. At each heat input increment the temperature of the evaporator surface was allowed to reach steady state. In addition, the effect of orientation on the FPHPs was evaluated by repeating the experimental measurements at tilt angles of 0°, 90°, and 180°. For comparison, further experimental tests were conducted on a 1 mm and 3 mm thick solid copper base plates under identical controlled conditions. In all tested samples, the operating temperature was measured at the heat source, T_H, evaporator plate corners T_{corner1} and T_{corner2}, and at the condenser surface, T_{cond}.

3.1. Solid Copper Base Plate Shelves. The initial tests of two solid copper plates of 45 mm × 45 mm and a thickness of 1 mm and 3 mm were carried out to provide a benchmark data which the thermal performance of the FPHPs was compared to. Results of these tests are shown in Figure 6, where it can be seen that for the same heat dissipation rates the temperature of the heat source in the 1 mm thick copper base is higher than that of the 3 mm thick copper base, particularly at high heat dissipation rates. For example, at a heat dissipation rate of 80 W, the recorded temperature, T_H, is 84°C and 73°C for the 1 mm and 3 mm thick base plates, respectively. Similarly, the temperature gradients between the heat source and the two far end corners, $\Delta T_{H\text{-corner}}$, and between the heat source and the heat sink, $\Delta T_{H\text{-cond}}$, are approximately 15°C higher for the 1 mm thick copper base than for its 3 mm thick counterpart. This shows that the 3 mm thick copper base plate has superior heat-spreading properties as predicated in the CFD simulation results.

3.2. Screen Mesh Wick Miniature FPHP. The procedure for evaluating the thermal performance of the screen mesh wick FPHP was similar to that presented in previous case with additional experimental measurements to assess the effect of orientation at tilt angles of 0°, 90°, and 180°. The measured temperature changes at the heat source and across the evaporator surface are shown in Figures 7(a) and 7(b). These show that at 0° and 90° tilt angles the FPHP performance is only comparable to that of the 1 mm thick solid copper base. For example at high-heat dissipation rates (80 W), the temperature of the heat source approaches 90°C and a large temperature gradient (30 to 40°C) appears across the evaporator surface and between the heat source and heat sink, $\Delta T_{H\text{-cond}}$. The thermal performance of the heat pipe has improved marginally for a tilt angle of 180° (gravity assisted wick capillary forces), but it remains that the 3 mm solid copper base plate performed better. This unexpected poor thermal performance may be attributed to the process of fabrication in which poor contact between the fine screen mesh and the inner evaporator wall could have prevented liquid circulation, leading to a high interfacial thermal resistance.

3.3. Sintered Copper Powder Wick FPHP. The sintered wick FPHP thermal performance is shown in Figures 8(a) and 8(b). It can be seen that for a heat dissipation rate of 80 W the measured temperature of the heat source at a tilt angle of 0° is 69°C, which is lower by 15°C and 5°C compared to the 1 mm and 3 mm copper base plates, respectively. For a tilt angle of 180° the temperature of the heat source has dropped even further to 61°C, an improvement of 12°C compared to the 3 mm copper base plate. Similarly, the measured temperature gradients $\Delta T_{H\text{-cond}}$ and $\Delta T_{H\text{-corner}}$ are 6°C and 5°C lower than that of the 3 mm copper base plate for a tilt angle of 0° and 10°C and 8°C for a tilt angle of 180°, respectively.

The high-thermal performance of the sintered wick miniature is due to high heat conduction and spreading capability of the sintered wick compared to a simple monolithic solid copper base plate or screen mesh wick FPHP.

4. Evaluation of Bulk and Thermal Spreading Resistance

The effective thermal resistance of an electronics component mounted on a PCB is the sum of a one-dimensional bulk resistance and a thermal spreading resistance. The one-dimensional bulk thermal resistance is expressed as follows [4, 20, 21]:

$$R_b = \frac{T_H - T_{\text{cond}}}{\dot{Q}_H}. \tag{4}$$

The thermal spreading resistance is associated, however, with discrete heat-generating components when mounted on a cold base plate, as found in electronics packages. The thermal spreading resistance characterises the ability of a base plate to spread the heat uniformly across the base plate surface (or the evaporator surface in the case of FPHP). The thermal spreading resistance could be of a similar magnitude to the one-dimensional bulk resistance in some designs of heat exchangers. Hence, its omission can lead to significant errors in estimating the temperature of a PCB, resulting in components overheating and failing prematurely. The thermal spreading resistance, R_{sp}, is computed using the following expression [21]:

$$R_{\text{sp}} = \frac{T_H - (T_{\text{corner1}} + T_{\text{corner2}})/2}{\dot{Q}_H}. \tag{5}$$

The variation of the one-dimensional bulk and thermal spreading resistances for the tested copper base plates and miniature FPHPs are shown in Figure 9. It can be seen that for heat dissipation rates of up to 40 W, the sintered wick heat pipe and the 3 mm thick copper base plate have comparable thermal performances in that both the one-dimensional and spreading thermal resistances are of similar magnitude. For higher heat dissipation rates, however, the advantage of a sintered wick FPHP becomes more apparent as the one-dimensional bulk and thermal spreading resistances are lower compared to other designs.

Finally, the uncertainty error of calculating the one-dimensional bulk and thermal spreading resistances is estimated from the measured data and the accuracy of the instruments used in the experiments. The accuracy of the T-type thermocouples is 0.5°C while the average error for power supply reading (wattmeter) is estimated at 2.3 W. Therefore, using the single sample analysis [22], the relative uncertainty error of the thermal resistance is calculated as follows:

$$e_R = \sqrt{\left(\frac{e_T}{\Delta T}\right)^2 + \left(\frac{e_Q}{\dot{Q}_H}\right)^2}. \tag{6}$$

It was assumed that the electrical power input to the heater block was fully dissipated as heat energy and that heat loss by convection and radiation from the test sample was negligible. The relative uncertainty error calculation of the thermal resistances has been limited to the case of the sintered wick FPHP, as shown in Table 3. The uncertainty calculation of the FPHP thermal resistance decreases from 13.6% to 3.8% for heat input rates of 20 W and 80 W, respectively. Although the average reading accuracy of the wattmeter is 2.3 W, the reading scale is nonlinear and the error of measurement is highest at low end of the scale, leading to large uncertainty of the measured thermal resistance for a heat rate input of 20 W.

5. Conclusion

This work investigated the thermal performance of a miniature FPHPs with sintered and screen mesh wicks for application in electronics cooling. The thermal performance of the FPHPs was further compared to that of copper solid base plates 1 mm and 3 mm thick. The ability of each sample to dissipate heat was evaluated by measuring the temperature distribution on the mounting surface and the temperature gradient between the heat source and heat sink. The main findings can be summarised as follows.

(i) The CFD results of predicting that the sintered wick FPHP would perform better than other arrangements were in good agreement with the experimental measurements.

(ii) It was found that the 3 mm thick copper base plate thermal performance surpasses that of the 1 mm and achieves higher heat conduction and spreading performance than the screen mesh wick FPHP.

(iii) The 3 mm thick copper base can perform adequately with heat dissipation rates of up to 40 W.

(iv) For heat dissipation rates higher than 40 W, the sintered wick FPHP outperforms the 3 mm copper base plate and its application would justify its high cost.

(v) The temperature measured on the evaporator surface of the sintered wick FPHP shows that there is no sign of liquid dry-out conditions in the wick for the range of heat dissipation rates.

(vi) The orientation of the sintered wick FPHP had marginal effect on its performance.

Acknowledgments

The authors wish to thank EPSRC (Engineering and Physical Sciences Research Council) for its financial support of the project under Grant EP/P500389/1 and Thermacore Europe Ltd for providing financial and technical help.

References

[1] D. A. Reay and P. A. Kew, *Heat Pipes: Theory, Design and Applications*, Butterworth-Heinemann, New York, NY, USA, 5th edition, 2006.

[2] M. Groll, "Heat pipe research and development in western Europe," *Heat Recovery Systems and CHP*, vol. 9, no. 1, pp. 19–66, 1989.

[3] A. Basiulis, H. Tanzer, and S. McCabe, "Thermal management of high power PWB's through the use of heat pipe substrates," in *Proceedings of the 6th Annual International Electronics Packaging Conference*, vol. 6, p. 501, San Diego, Calif, USA, 1986.

[4] M. Adami and B. Yimer, "Development and evaluation of a planar heat pipe for cooling electronic systems," *Chemical Engineering Communications*, vol. 90, no. 1, pp. 57–74, 1990.

[5] S. W. Kang, S. H. Tsai, and H. C. Chen, "Fabrication and test of radial grooved micro heat pipes," *Applied Thermal Engineering*, vol. 22, no. 14, pp. 1559–1568, 2002.

[6] C. Y. Liu, C. Y. Liu, K. C. Leong, Y. W. Wong, and F. L. Tan, "Performance study of flat plate heat pipe," in *Proceedings of the International Conference on Energy and Environment (ICEE)*, pp. 512–518, Begell House Inc., New York, NY, USA, 1996.

[7] A. Christensen and S. Graham, "Thermal effects in packaging high power light emitting diode arrays," *Applied Thermal Engineering*, vol. 29, no. 2-3, pp. 364–371, 2009.

[8] X. Y. Huang and C. Y. Liu, "The pressure and velocity fields in the wick structure of a localized heated flat plate heat pipe," *International Journal of Heat and Mass Transfer*, vol. 39, no. 6, pp. 1325–1330, 1996.

[9] W. Qin and C. Y. Liu, "Liquid flow in the anisotropic wick structure of a flat plate heat pipe under block-heating condition," *Applied Thermal Engineering*, vol. 17, no. 4, pp. 339–349, 1997.

[10] B. K. Tan, X. Y. Huang, T. N. Wong, and K. T. Ooi, "A study of multiple heat sources on a flat plate heat pipe using a point source approach," *International Journal of Heat and Mass Transfer*, vol. 43, no. 20, pp. 3755–3764, 2000.

[11] R. Sonan, S. Harmand, J. Pellé, D. Leger, and M. Fakès, "Transient thermal and hydrodynamic model of flat heat pipe for the cooling of electronics components," *International Journal of Heat and Mass Transfer*, vol. 51, no. 25-26, pp. 6006–6017, 2008.

[12] A. P. Bakke, "Light weight rigid flat plate heat pipe utilizing copper foil container laminated to heat treated Aluminium plates for structural stability," US Patent No. 6679318 B2, 2004.

[13] J. H. Rosenfeld, N. J. Gernert, D. V. Sarraf, P. Wollen, F. Surina, and J. Fale, "Flexible heat pipe," US Patent No. 6446706 B1, 2002.

[14] Y. Koito, H. Imura, M. Mochizuki, Y. Saito, and S. Torii, "Numerical analysis and experimental verification on thermal fluid phenomena in a vapor chamber," *Applied Thermal Engineering*, vol. 26, no. 14-15, pp. 1669–1676, 2006.

[15] G. Carbajal, C. B. Sobhan, G. P. Bud Peterson, D. T. Queheillalt, and H. N. G. Wadley, "A quasi-3D analysis of the thermal performance of a flat heat pipe," *International Journal of Heat and Mass Transfer*, vol. 50, no. 21-22, pp. 4286–4296, 2007.

[16] R. Ranjan, J. Y. Murthy, and S. V. Garimella, "Analysis of the wicking and thin-film evaporation characteristics of microstructures," *Journal of Heat Transfer*, vol. 131, no. 10, pp. 1–11, 2009.

[17] A. Bhattacharya, V. V. Calmidi, and R. L. Mahajan, "Thermophysical properties of high porosity metal foams," *International Journal of Heat and Mass Transfer*, vol. 45, no. 5, pp. 1017–1031, 2002.

[18] J. Thayer, "Analysis of a heat pipe assisted heat sink," in *Proceedings of the 9th International FLOTHERM Users Conference*, Orlando, Fla, USA, October 2000.

[19] B. Xiao and A. Faghri, "A three-dimensional thermal-fluid analysis of flat heat pipes," *International Journal of Heat and Mass Transfer*, vol. 51, no. 11-12, pp. 3113–3126, 2008.

[20] R. Boukhanouf, A. Haddad, M. T. North, and C. Buffone, "Experimental investigation of a flat plate heat pipe performance using IR thermal imaging camera," *Applied Thermal Engineering*, vol. 26, no. 17-18, pp. 2148–2156, 2006.

[21] Y. S. Muzychka, M. R. Sridhar, M. M. Yovanovich, and V. W. Antonetti, "Thermal spreading resistance in multilayered contacts: applications in thermal contact resistance," *Journal of Thermophysics and Heat Transfer*, vol. 13, no. 4, pp. 489–494, 1999.

[22] S. J. Kline and F. A. McClintock, "Describing uncertainties in single sample experiments," *Mechanical Engineering*, vol. 75, pp. 3–8, 1953.